Intercalation of sodium and heavy alkali metals into graphenic foams

Lucie Speyer, Sébastien Fontana, Sébastien Cahen, Claire Hérold

Intercalation of sodium and heavy alkali metals into graphenic foams

Lucie Speyer, Sébastien Fontana, Sébastien Cahen, Claire Hérold

Institut Jean Lamour, UMR 7198 CNRS – Université de Lorraine, Campus ARTEM,

2 allée André Guinier, BP 50840, 54011 Nancy cedex, France

Lucie Speyer : lucie.speyer@univ-lorraine.fr *(corresponding author)*

Sébastien Fontana : sebastien.fontana@univ-lorraine.fr

Sébastien Cahen : sebastien.cahen@univ-lorraine.fr

Claire Hérold : c.herold@univ-lorraine.fr

Abstract

Most of alkali metals are well-known to easily intercalate into graphite to form stage-1 graphite intercalation compounds (GIC) whose structure and physical properties have been extensively studied. This work is focused on the intercalation of potassium, sodium and cesium into graphenic foams prepared by a solvothermal-based process. The as-obtained samples are analyzed by means of X-ray diffraction and Raman spectroscopy, and reveal a double phenomenon: the intercalation of alkali metals between the interplanar spaces of the multi-layer graphene stackings, and their sorption into the porosity of the host sample. This kind of behavior has already been reported when studying the reactivity of alkali metals with disordered carbon. Interestingly, our study shows a low stage intercalation in the case of sodium. Moreover, the dispersion of the potassium-intercalated samples into a polar solvent leads to a few-layer graphene dispersion stable for months.

Keywords

Graphenic foam – Intercalation – Alkali metals – Raman spectroscopy – Graphene dispersions

1. Introduction

Thanks to its lamellar structure, graphite can host various chemical species into its interplanar spaces to form graphite intercalation compounds (GIC). Graphite-alkali metals are the first known GIC [1]. Due to their well-adapted melting point and vapor pressure, most of alkali metals easily intercalate into graphite by chemical vapor

transport to form bulk and saturated GIC: crystal structures of LiC_6, KC_8, RbC_8 and CsC_8 first stage GIC are well-known [2 – 5]. In the particular case of sodium, owing to a very weak interaction between sodium and graphite [6], only pure stage 5 to 8 compounds are obtained [7, 8] whereas the first stage GIC NaC_8 can only be stabilized under high pressure [9]. Intercalation induces new properties in respect with those of pristine host material. For example, in the case of potassium, rubidium and cesium, stage-1 GIC become superconducting at low temperature [10]. Furthermore, intercalation into graphite is the founding concept of alkali-ion batteries, which makes GIC a fundamental topic in the current energy transition context.

More recently, with the well-known emergence of carbon nanomaterials, intercalation of alkali metals into graphene-based structures constituted the subject of some studies. Indeed, GIC obtained using few- or multi-layer graphene show different properties from those of bulk GIC. For instance, the influence of intercalation on band structure and optical and electronic properties of few-layer graphene has been explored [11 – 15]. Interestingly, superconductivity is also modified when the GIC are few-layer-thick only. For example, bulk LiC_6 does not show any superconducting properties but lithium adsorbed on monolayer graphene exhibits a superconducting transition at several K [16, 17]. In the case of KC_8, a few-layer GIC is reported with a critical temperature which is an order of magnitude above the temperature for the bulk compound [18].

Besides the fundamental interest of the intercalation into nanocarbons, this topic is also relevant for the context of energy applications, especially in the field of alkali-ion batteries. Some studies report higher lithium storage capacities when graphite, the classical anode material, is replaced by nanocarbons as for instance crumpled graphene nanosheets [19 – 21]. The better capacity is attributed to the reactivity of lithium with graphene edges and defects. Moreover, in order to overcome the disadvantage of lithium

availability, sodium-ion batteries appear as an appropriate alternative [22]. Indeed, sodium is an abundant and low-cost element and, being an alkali metal too, its properties are close to those of lithium. As intercalation of sodium into graphite is not efficient, other anode materials have to be investigated. Hard carbons are promising candidates: their partially disordered structure allows a better intercalation of sodium into the small graphitized domains, and a sorption of sodium inside the porosity [8, 23, 24]. Both phenomena appear on the galvanostatic charge/discharge curves of hard carbon electrodes versus sodium [23, 24]. Such disordered carbon structures are also promising for potassium-ion batteries, for which sodium and potassium storage mechanisms are reported to be the same [25].

Furthermore, GIC can be employed as precursors for graphene fabrication. Indeed, intercalation are redox reactions: a charge transfer between the host and the intercalant provides, in the case of alkali metals, a negative charge of the graphene layers and a positive chargie of the metal layers. The dissolution of a GIC in a polar solvent can therefore exfoliate the material and stabilize the individualized graphene layers in solution [26].

This work is focused on the intercalation of three alkali metals, sodium, potassium and cesium, into multi-layer graphenic foams obtained by a solvothermal-based process. These foams exhibit high structural quality as same as very high specific surface areas [27]. Intercalation of alkali metals in partially disordered and highly porous carbon materials is studied from a fundamental point of view and regarding the aforementioned potential applications. Intercalated graphenic foams are studied by X-ray diffraction and by Raman spectroscopy, which reveal, even in the case of sodium, a notable intercalation and entrapment of the alkali metal in the porosity of the sample. Considering the potentiality of intercalated samples for the preparation of graphene

dispersions, we report in a second part the dissolution of intercalated graphenic foams in a polar solvent. Dimethylsulfoxide (DMSO), with an electric dipole moment of 4.06 D, has shown a great efficiency to debundle, on the same principle as for GIC, carbon nanotubes samples intercalated with potassium [28]. Moreover, the use of multi-layer graphene instead of bulk graphite could lead to a very low number of stacked graphene layers in the final suspension. By dispersion of a graphenic foam intercalated with potassium, we obtain graphene suspensions which are stable during several months.

2. Experimental

2.1. Intercalation into graphenic foams

Graphenic foams (denoted GF) are elaborated as described elsewhere, using a solvothermal reaction between ethanol and sodium followed by a pyrolysis under a nitrogen flow and a washing step [27]. The pyrolysis conditions are 850°C and 8h and have been found to be optimal for the structural quality and the porosity of the foam. Graphenic foams, placed in a Pyrex ampoule, are first degassed at 400°C under secondary vacuum during several hours. They are transferred into a glove box under purified argon atmosphere and placed at the extremity of a Pyrex tube. A piece of alkali metal is then introduced in the tube, at several centimeters from GF. In all cases, metals are introduced in large excess against graphite in order to obtain saturated compounds. The tube is sealed under secondary vacuum, then placed in a horizontal tubular furnace and heated during 10 days. A temperature gradient of several degrees has to be between alkali metal and graphene foam, the latter being a little hotter. The hot temperature is 210°C for sodium, 180°C for potassium and 160°C for cesium. Once the reaction is

completed, the tube is reintroduced in the glove box and open to recover the intercalated sample. The samples are named GF-K, GF-Cs and GF-Na.

2.2. Dispersion

As an example, the GF-K sample has been dispersed. In a glove box under purified argon atmosphere, a small quantity of GF-K is introduced in a vial which is sealed with Parafilm and transferred in a glove bag under nitrogen atmosphere. Anhydrous DMSO is then added in the vial with a syringe. The concentration of the dispersion is about 2 $mg.mL^{-1}$ and the sample is denoted as GF-K-disp.

2.3. Characterization

Transmission electron microscopy is carried out with a Jeol ARM 200F microscope operating at 200 keV. Raw graphenic foam is dispersed in ethanol, and the dispersion of intercalated sample GF-K-disp is analyzed as prepared. A drop of dispersion is deposited on a copper grid with a holey carbon film. For GF-K-disp, the grid is rapidly introduced into the microscope in order to limit the air exposure.

X-ray diffraction is carried out with a Bruker D8 Advance diffractometer ($\lambda(Mo_{K\alpha 1})$ = 0.70930 Å) in a Bragg-Brentano $\theta/2\theta$ configuration on an angular range 5-30°. In glove box, samples are introduced in Lindemann glass capillaries (1.5 mm diameter). XRD pattern are recorded for 24 hours with 50kV and 45 mA X-ray beam conditions.

Raman spectroscopy is performed with a Jobin Yvon HR800 LABRAM spectrometer with a λ = 633 nm radiation on a spectral range 850-1800 cm^{-1} and 2500-2850 cm^{-1} for GF, and 400-2800 cm^{-1} for intercalated samples. Prior to analysis, GF is dispersed in

ethanol and a drop of the dispersion is deposited on a glass slice. Intercalated samples are placed under purified argon atmosphere in quartz cells which are sealed under a low helium partial pressure. A power filter is applied in order to avoid the damaging of the samples by the laser beam: microscopic observations of the samples and recorded spectra on the same area assess the absence of degradation.

Adsorption isotherms (N_2 77 K) are collected using a Micromeritics ASAP 2020 adsorption apparatus. GF is first degassed at 400°C during 12h. Specific surface areas and pore size distributions are calculated using the 2D-NLDFT model, well adapted for microporous samples [29]. BET surface areas adjusted with the Rouquerol correction [30] are given in comparison since it is the most frequent model used in the literature.

3. Results and discussion

3.1. Description of the raw graphenic foam

The raw sample GF is a graphenic foam powder prepared by a solvothermal-based process. Transmission electron micrographs are shown Fig. 1.

Fig. 1a shows the typical structure of the graphenic foam used for this study. The multi-layer stacking and the graphenic hexagonal lattice can be observed on micrographs 1b and 1c. Fig. 2 presents the X-ray diffractogram and the Raman spectrum of the sample. According to X-ray diffraction, hexagonal graphite is the major phase constituting the sample. Other carbon structures (turbostratic and orthorhombic) correspond to more disordered graphitic phases involving stacking faults [31], [32]. By applying the Debye-Scherrer equation to the (002) peak of hexagonal graphite (12°), the average crystallite size along **c** axis is 4.3 nm, so the average number of stacked graphene layers is 13. A

small fraction of sodium carbonate (12.7wt% according to TGA measurements, not shown here) is entrapped into the cavities of the graphenic foam structure, which hinders its complete elimination during the washing step [33]. The Raman spectrum shows the typical D, G, D' and 2D bands of graphenic and graphitic materials, as same as two additional A and B bands related to disordered carbons [27]. After deconvolution of the first region of the spectrum, the I_D/I_G ratio is equal to 0.88 and the Full-Width at Half Maximum (FWHM) of the G peak is 30 cm^{-1} only, confirming the high structural quality of the sample first evidenced by TEM observations. The N_2 adsorption isotherm and corresponding 2D-NLDFT pore size distribution are plotted Fig. 3.

The adsorption isotherm is a combination of type I, II and IV isotherms using the IUPAC classification [34], indicating the presence of macropores (multi-layer graphene surfaces, larger graphenic foam cavities), mesopores (smaller graphenic foam cavities or intergranular mesoporosity) and micropores (adsorption on disordered carbon). The mesoporous and microporous nature of the sample is confirmed by the pore size distribution. The 2D-NLDFT model provides a value of 1620 $m^2.g^{-1}$ for the specific surface area (the BET surface area is 2240 $m^2.g^{-1}$) and a 1.6 $cm^3.g^{-1}$ value for the pore volume, which are very elevated values due to the structure of the graphenic foam.

3.2. Intercalation into the graphenic foam

The three samples keep their powdery nature after reaction with the alkali metals. As GF-Na remains as black as the raw GF sample, GF-K and GF-Cs present a brown color, which can be related to the golden-brown color of bulk first-stage KC_8 and CsC_8 compounds. This first observation indicates that, at least for potassium and cesium, a

reaction between the alkali metal and the graphenic foam has occured. Table 1 reports, for each sample, the weight uptake after reaction and the C/metal atomic ratio.

For each alkali metal, the sample undergoes an important weight uptake after reaction. The corresponding C/metal atomic ratios, quite similar for the three samples, are much larger than the value of 8 observed for the first-stage GIC. Then, we assume that the intercalation of the alkali metal into the multi-layer stackings of the graphenic foam is accompanied by a sorption of metal into its porosity. It is worth noting that the C/metal atomic ratio for GF-Na is the same as for GF-K and GF-Cs, even if the intercalation has not caused any change of color. X-ray diffractograms of GF-K, GF-Cs and GF-Na are given Fig. 4, Fig. 5 and Fig. 6.

For each sample, the diffractograms may be indexed with the most stable graphite intercalation compound corresponding to the metal (stage-1 for K and Cs and stage 8 for Na), the metal and pristine graphitic structures. It is worth noting that the interpretation of the X-ray diffraction experiment is difficult given the peak widths and the possible overlap of the reflections corresponding to distinct phases. However, the supposed presence of KC_8, CsC_8, NaC_{64} and the alkali metals is consistent with the C/metal atomic ratios. The latter indicates both intercalation and sorption of the metal and other characterization techniques have been used in order to confirm this assumption. Raman spectroscopy is a powerful tool for the analysis of GIC [35]. At first, Raman spectra of GF-K and GF-Cs are plotted Fig.7. For both samples, several spectra have been recorded on different areas and are similar, indicating homogeneous materials.

Raman spectra of GF-K and GF-Cs are very similar. First, both spectra present a band around 560 cm^{-1} denoted C_z band and related to the vibrations along **c** axis. This band is only observed for stage-1 graphite intercalation compounds. Its intensity increases

together with the size of the intercalated atom, which is clearly observed here [36]. The 2D band observed for the raw graphene foam completely disappears for the samples GF-K and GF-Cs, which indicates a stage-1 intercalation too. Indeed, the presence of intercalate in each interlayer space of graphenic stacking hinders the double resonance process which gives rise to the 2D band in graphenic materials [14]. The last modification of the spectra is the replacement of the A, B, D, G and D' bands by a very broad and asymmetric signal. This feature is once again a signature of stage-1 GIC and can be decomposed into four components [37, 38]. Figure 8 shows the decomposition of the 1200-1800 cm^{-1} region of the spectra of GF-K and GF-Cs. The parameters of the different components are listed on Table 2.

As reported in the literature, the 1200-1800 cm^{-1} region of both samples can be decomposed into four components. The D and GD bands are Lorentzian curves related to intrinsic defects of the carbon host structure even after intercalation. The E_{2g1} and E_{2g2} bands are Breit-Wigner-Fano (BWF) signals, related to the presence of the intercalate. The asymmetric shape of these bands is due to a coupling between the electronic states of the graphene layers and the alkali metal. The position and FWHM of the four bands are quite similar for GF-K and GF-Cs, only the relative intensities of the bands vary. These differences are due to the nature of the metal intercalated into the samples [37, 38].

Then, from the presence of the C_z band, the shape of the 1200-1800 cm^{-1} region and the absence of the 2D band, Raman spectroscopy assesses a stage-1 intercalated GF-K and GF-Cs phases. These results are in accordance with the chemical composition of the samples, and with their brown color too.

Fig. 9 presents Raman spectra recorded on several particles (from 1 to 10 μm) of the sample GF-Na. Contrary to the samples GF-K and GF-Cs, Raman spectra for GF-Na depend on the zone where they are recorded.

For smaller particles (spectra (a) and (b)), the D-G region clearly shows the emergence of the D and G bands of the pristine sample. Between them, an asymmetric band could be discerned and may correspond to the presence of a little amount of intercalated sodium. It is interesting to note that for these two spectra, a coexistence of the C_z band and the 2D band is observed. It could be attributed to small domains of stage-1 NaC_8, giving rise to the C_z band, and small domains of pristine graphite or high stage intercalation compound which give rise to the 2D band. It could be possible that, due to the peculiarity of the interaction between sodium and graphite, the C_Z and 2D bands may coexist in the stage-1 compound. In the case of the large particle (spectrum (c)), the C_z band is absent, the 2D band is quite intense and in the 2D region, the D and G bands are clearly observed. Large particles are poorly intercalated, and sodium is mainly intercalated in smaller particles. It could explain the lack of coloration of the sample after reaction with sodium. In this latter case, Raman spectra indicate low stage compounds with possibly stage-1 domains, in accordance with the literature which reports a better intercalation of sodium in partially disordered carbon materials [8,23,24]. Raman results are in accordance with XRD results, showing the probable presence of pristine graphite and high-stage intercalation compounds. NaC_8 does not seem to be present from the diffractogram but, as mentioned earlier, low-stage compounds are formed from small particles, which could explain that their detection is disadvantaged compared to larger and poorly-intercalated particles.

The difference of behavior between sodium and both other alkali metals is attributed to the peculiar interaction between sodium and graphitic carbon materials which has been

found to be very weak [6]. It is not a matter of atomic size, because sodium is the smallest of the atoms studied in this work. Except sodium, all alkali metals, which are very electropositive, easily intercalate into graphite by a simple chemical vapor transport phenomena [2 – 5]. However, in the case of sodium, electronegativity is not a relevant parameter: the electronegativity of sodium is intermediate between those of lithium and potassium, and lithium and potassium form stable stage-1 compounds as sodium does not. In the case of graphenic foams, the intrinsic structural disorder of the host structure allows the formation of low-stage compounds with possible stage-1 regions, but the case of sodium still differs from potassium and cesium for which homogeneous stage-1 compounds are evidenced.

The adsorption phenomenon is likely to be the same for all alkali metals, since their size allows them an access to the whole porosity of the foams. The particular reactivity of sodium regarding the intercalation seems to be the major reason explaining the results of this study.

3.3. Dispersion of the potassium intercalated foam

Figure 10 presents a photograph of the sample GF-K-disp just after its preparation, and eight months after.

The photograph (a) shows an uniform black suspension and indicates the efficient dispersion of the sample GF-K in DMSO. Eight months after the preparation, in spite of a small decantation, the suspension remains stable and shows the typical brown color of suspended graphene flakes. TEM micrographs of the sample are presented on Fig. 11. The micrograph (a) shows the same structure as the raw graphenic foam. Very thin and flat zones can be observed, as on micrograph (b), indicating the local efficiency of the

intercalation-dispersion process. This kind of structures has never been detected on the pristine graphenic foam and are then directly related to this further treatment of the sample. On these thin zones, only a very few number of graphene layers are stacked, as shown on micrograph (c) where bilayer graphene is evidenced. As a reminder, the multi-layer graphene stacking of the raw sample GF is constituted of an average number of 13 layers. These observations confirm an efficient dispersion of GF-K in DMSO.

4. Conclusions

This study is focused on the intercalation of alkali metals in multi-layer porous graphenic foams and the elaboration of graphene suspensions from the as-prepared intercalated samples. After reaction with potassium, cesium or sodium vapor, a large mass uptake is observed, indicating the occurrence of two phenomena: the sorption of the metal into the porosity of the foam, and its intercalation in the multi-layer graphene stackings. These phenomena lead to the obtaining of metal-rich samples.

In the case of potassium and cesium, an homogeneous stage-1 compound is clearly evidenced by Raman spectroscopy. Then, alkali metals completely fill the interplanar spaces and the porosity of the foams, in accordance with the mass variations. The case of sodium is especially interesting: the intercalation of this element into graphite is known to be very inefficient relative to the other alkali metals. Indeed, the intercalation of sodium into our graphenic foam is inhomogeneous but when it occurs, Raman spectra seem to indicate saturated intercalated zones. This efficient intercalation is due to the small lateral size of the particles, the intrinsic defects of the material, and the low number of stacked graphene layers. These observed phenomena are similar to those observed in alkali-ion batteries [23-25]. It is worth noting that high specific areas are

not desirable for electrode materials in alkali-ion batteries, since an important passivation layer would form at the electrode surface during the first electrochemical cycle and would lead to an large capacity fading [24]. A modification of the porosity of the sample would be adapted in order to optimize the relative importance of intercalation and sorption of sodium: the possibility of this modification has been proven by modifying, for example, the precursor alcohol used in the solvothermal-based process [39]. Besides a possible optimization of the specific surface area by changing the alcohol, hollow structures comparable to graphenic foams have been reported to present good performances as electrode materials for batteries [40]. Especially in the case of potassium, this kind of structure is described as efficient to buffer the volumic variations of the electrode due to the size of potassium atoms [41]. Then, the modification of the elaboration conditions of solvothermal-based graphenic foams could be a possible work trail towards materials for electrochemical energy storage.

In a second part of the study, graphenic foam intercalated with potassium has been dispersed in DMSO, a polar solvent, in order to exfoliate the graphene layers. Graphene suspensions which are stable during several months have been prepared and transmission electron microscopy shows a local efficient exfoliation. It could be interesting to adapt the concentration of the dispersions and to perform an ultrasonication to improve the exfoliation ratio, given these promising results.

References

[1] K. Fredenhagen, G. Cadenbach, Z. Anorg. Allg. Chemie 158 (1926) 249-263. https://doi.org/10.1002/zaac.19261580122

[2] A. Hérold, Bull. Soc. Chim. Fr. 187 (1955) 999-1012.

[3] P. Lagrange, D. Guérard, A. Hérold, Ann. Chim. Fr. 3 (1978) 143-159.

[4] P. Lagrange, D. Guérard, M. El Makrini, A. Hérold, C. R. Acad. Sc. Paris 287 (1978) 179-182.

[5] D. Guérard, P. Lagrange, M. El Makrini, A. Hérold, Carbon 16 (1978) 285-290. https://doi.org/10.1016/0008-6223(78)90044-1

[6] D.P. DiVincenzo, E.J. Mele, Phys. Rev. B 32 (1985) 2538-2553. https://doi.org/10.1103/PhysRevB.32.2538

[7] R.C. Asher, S.A. Wilson, Nature 181 (1958) 409-410. https://doi.org/10.1038/181409a0

[8] A. Métrot, D. Guérard, D. Billaud, A. Hérold, Synth. Metals 1 (1979) 363-369. https://doi.org/10.1016/0379-6779(80)90071-5

[9] V.A. Nalimova, V.V. Avdeev, K.N. Semenenko, Mat. Sci. Forum 91-93 (1992) 11-16. https://doi.org/10.4028/www.scientific.net/MSF.91-93.11

[10] N.B. Hannay, T.H. Geballe, B. T. Matthias, K. Andres, P. Schmidt, D. MacNair, Phys. Rev. Lett. 14 (1965) 225-226. https://doi.org/10.1103/PhysRevLett.14.225

[11] E. Pollak, B. Geng, K.J. Jeon, I.T. Lucas, T.J. Richardson, F. Wang, R. Kostecki, Nano Lett. 10 (2010) 3386-3388. https://doi.org/10.1021/nl101223k

[12] E. Lee, K.A. Persson, Nano Lett. 12 (2012) 4624-4628. https://doi.org/10.1021/nl3019164

[13] N. Jung, B. Kim, A.C. Crowther, N. Kim, C. Nuckolls, L. Brus, ACS Nano 5 (2011):5708-16. https://doi.org/10.1021/nn201368g

[14] J.C. Chacon-Torres, L. Wirtz, T. Pichler, ACS Nano 7 (2013) 9249-9259. https://doi.org/10.1021/nn403885k

[15] J. Algdal, T. Balasubramanian, M. Breitholz, T. Kihlgren, L. Wallden, Surf. Sci. 601 (2007) 1167-1175. https://doi.org/10.1016/j.susc.2006.12.039

[16] G. Profeta, M. Calandra, F. Mauri, Nature Phys. 8 (2012) 131-134. https://doi.org/10.1038/nphys2181

[17] B.M. Ludbrook, G. Levy, P. Nigge, M. Zonno, M. Schneider, D.J. Dvorak, C. N. Veenstra, S. Zhdanovich, D. Wong, P. Dosanjh, C. Strasser, A. Stöhr, S. Forti, C. R. Ast, U. Stark, A. Damascelli, Proc. Natl. Acad. Sci. USA 112 (2015) 11795-11799. https://doi.org/10.1073/pnas.1510435112

[18] M. Xue, G. Chen, H. Yang, Y. Zhu, D. Wang, J. He, T. Cao, J. Am. Chem. Soc. 134 (2012) 16536-16539. https://doi.org/10.1021/ja3003217

[19] E. Yoo, J. Kim, E. Hosono, H. Zhou, T. Kudo, I. Honma, Nano Lett. 8 (2008) 2277-2282. https://doi.org/10.1021/nl800957b

[20] P. Guo, H. Song, X. Chen, Electrochem. Comm. 11 (2009) 1320-1324. https://doi.org/10.1016/j.elecom.2009.04.036

[21] J. Hassoun, F. Bonaccorso, M. Agostini, M. Angelucci, M.G. Betti, R. Cingolani M. Gemmi, C. Mariani, S. Panero, V. Pellegrini, B. Scrosati, Nano Lett. 14 (2014) 4901-4906. https://doi.org/10.1021/nl502429m

[22] M.D. Slater, D. Kim, E. Lee, C.S. Johnson, Adv. Funct. Mater. 23 (2013) 947-958. https://doi.org/10.1002/adfm.201200691

[23] E. Irisarri, A. Ponrouch, M.R. Palacin, J. Electrochem. Soc. 162 (2015) 2476-2482. https://doi.org/10.1149/2.0091514jes

[24] D. Saurel, B. Orayech, B. Xiao, D. Carriazo, X. Li, T. Rojo, Adv. Energy Mater. 8 (2018) 1703268. https://doi.org/10.1002/aenm.201703268

[25] Z. Jian, Z. Xing, C. Bommier, Z. Li, X. Ji, Adv. Energy Mater. 6 (2016) 1501874. https://doi.org/10.1002/aenm.201501874

[26] A. Catheline, L. Ortolani, V. Morandi, M. Melle-Franco, C. Drummond, C. Zakri, A. Pénicaud, Soft Matter 8 (2012) 7882-7887. DOI: 10.1039/C2SM25960E

[27] L. Speyer, S. Fontana, S. Cahen, J. Ghanbaja, G. Medjahdi, C. Hérold, Solid State Sci. 50 (2015) 42-51. https://doi.org/10.1016/j.solidstatesciences.2015.10.009

[28] E. Remy, C. Hérold, F. Valsaque, J.F. Marêché, S. Fontana, A. Desforges, S. Cahen, J. Ghanbaja, J. Gleize, B. Vigolo, J. Phys. Chem. C 117 (2013) 19245-19252. https://doi.org/10.1021/jp406396y

[29] J. Jagiello, P. Olivier, Carbon 55 (2013) 70-80. https://doi.org/10.1016/j.carbon.2012.12.011

[30] J. Rouquerol, D. Avnir, C.W. Fairbridge, D.H. Everett, J.M. Haynes, N. Pernicone, J.D.F. Ramsay, K.S.W. Sing, K.K. Unger, Pure Appl. Chem. 66 (1994) 1739-1758. https://doi.org/10.1515/iupac.66.0925

[31] P.D. Ownby, X. Yang, J. Liu, J. Am. Ceram. Soc. 75 (1992) 1876-1883. https://doi.org/10.1111/j.1151-2916.1992.tb07211.x

[32] J. Fayos, J. Solid State Chem. 148 (1999) 278-285. https://doi.org/10.1006/jssc.1999.8448

[33] L. Speyer, S. Fontana, S. Cahen, C. Hérold, Mater. Chem. Phys. 219 (2018) 57-66. https://doi.org/10.1016/j.matchemphys.2018.08.020

[34] K.S.W. Sing, D.H. Everett, R.A.W. Haul, L. Moscou, R.A. Pierotti, J. Rouquerol, T. Siemieniewska, Pure Appl. Chem. 57 (1995) 603-619. https://doi.org/10.1515/iupac.57.0007

[35] J.C. Chacon-Torres, L. Wirtz, T. Pichler, Phys. Status Solidi B 12 (2014) 2337-2355. https://doi.org/10.1002/pssb.201451477

[36] M.P.M. Dean, C.A. Howard, S.S. Saxena, P. Ellerby, Phys. Rev. B 81 (2010) 045405. https://doi.org/10.1103/PhysRevB.81.045405

[37] J.C. Chacon-Torres, A.Y. Ganin, M.J. Rosseinsky, Phys. Rev. B 86 (2012) 075406. https://doi.org/10.1103/PhysRevB.86.075406

[38] J.C. Chacon-Torres, T. Pichler, Phys. Status Solidi B 248 (2011) 2744-7. https://doi.org/10.1002/pssb.201100135

[39] L. Speyer, S. Fontana, S. Ploneis, C. Hérold, Micropor. Mesopor. Mat. 2017243 (2017) 254-262. https://doi.org/10.1016/j.micromeso.2017.02.035

[40] K. Tang, L. Fu, R. J. White, L. Yu, M. Titirici, M. Antonietti, J. Maier, Adv. Energy Mater. 2 (2012) 873-877. https://doi.org/10.1002/aenm.201100691

[41] J. C. Pramudita, D. Sehrawat, D. Goonetilleke, N. Sharma, Adv. Energy Mater. 7 (2017) 1602911. https://doi.org/10.1002/aenm.201602911

Tables

Table 1. Relative weight uptake during reaction and C/metal atomic ratio of samples GF-Na, GF-K and GF-Cs.

Sample	Relative weight uptake (%)	C/metal atomic ratio
GF-K	15.9	2.7
GF-Cs	31.3	2.8
GF-Na	20.0	2.5

Table 2. Position, FWHM, normalized intensity and q asymmetry factor of the components D, GD, E_{2g1} and E_{2g2} of the samples GF-K and GF-Cs.

	D band		E_{2g2} band		E_{2g1} band		GD band	
	GF-K	GF-Cs	GF-K	GF-Cs	GF-K	GF-Cs	GF-K	GF-Cs
Position (cm^{-1})	1255	1260	1367	1368	1466	1464	1536	1532
FWHM (cm^{-1})	53	70	80	79	78	85	90	75
Intensity (a. u.)	0.25	0.22	0.76	0.59	1	1	0.55	0.24
q	-	-	-3	-3	-3	-3	-	-

Figure captions

Fig. 1. Transmission electron micrographs of the sample GF.

Fig. 2. a) X-ray diffractogram ($\lambda(Mo_{K\alpha1})$ = 0.70930 Å) indexed with hexagonal graphite (PDF n° 04-007-2081), turbostratic carbons [30], orthorhombic carbon [31] and sodium carbonate (PDF n° 04-010-2762) ; b) Raman spectrum (λ = 633 nm) of the sample GF.

Fig. 3. Adsorption isotherm (N_2 77 K) and 2D-NLDFT pore size distribution of the sample GF.

Fig. 4. X-ray diffractogram ($\lambda(Mo_{K\alpha1})$ = 0.70930 Å) of the sample GF-K, indexed with KC_8 [3], K (PDF n° 04-013-3196), hexagonal graphite (PDF n° 04-007-2081) and turbostratic carbons [31].

Fig. 5. X-ray diffractogram ($\lambda(Mo_{K\alpha1})$ = 0.70930 Å) of the sample GF-Cs, indexed with CsC_8 [5], Cs (PDF n° 04-013-7469), hexagonal graphite (PDF n° 04-007-2081) and turbostratic carbons [31].

Fig. 6. X-ray diffractogram ($\lambda(Mo_{K\alpha1})$ = 0.70930 Å) of the sample GF-Na, indexed with NaC_{64} [7], Na (PDF n° 04-013-7469), hexagonal graphite (PDF n° 04-007-2081) and turbostratic carbons [31].

Fig. 7. Normalized Raman spectra (λ = 633 nm) of the samples GF-K and GF-Cs.

Fig. 8. Curve fitting of the Raman spectra of the samples GF-K and GF-Cs.

Fig. 9. Raman spectra (λ = 633 nm) recorded on a large particle (around 10 μm) and two small particles (around 1 μm) of the sample GF-Na.

Fig. 10. Photograph of the sample GF-K-disp just after its preparation (a) and 8 months after its preparation (b).

Fig. 11. Transmission electron micrographs of the sample GF-K-disp.

Figures

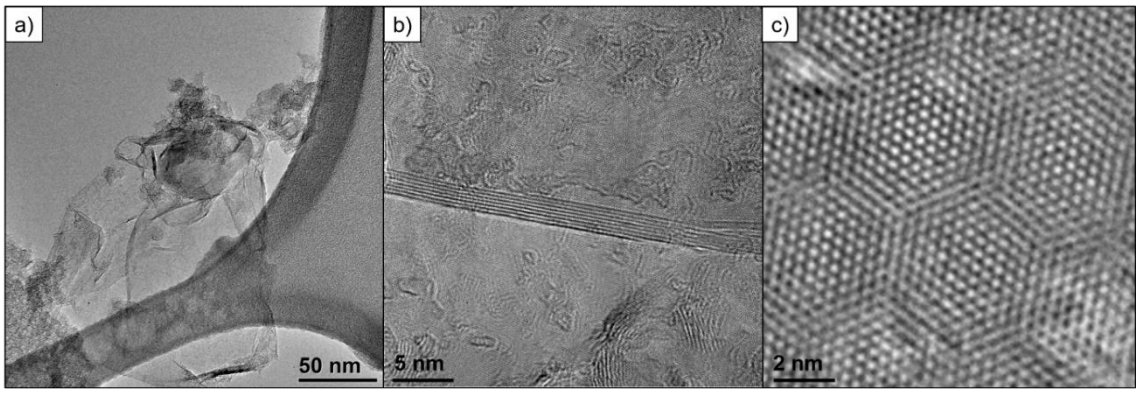

Fig 1

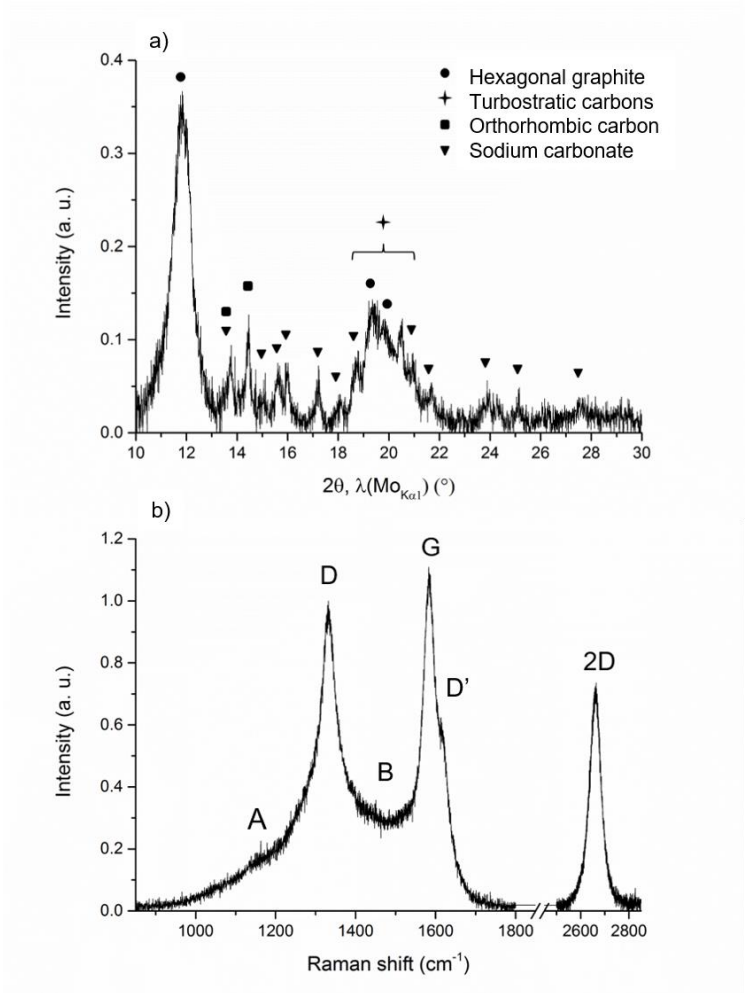

Fig 2

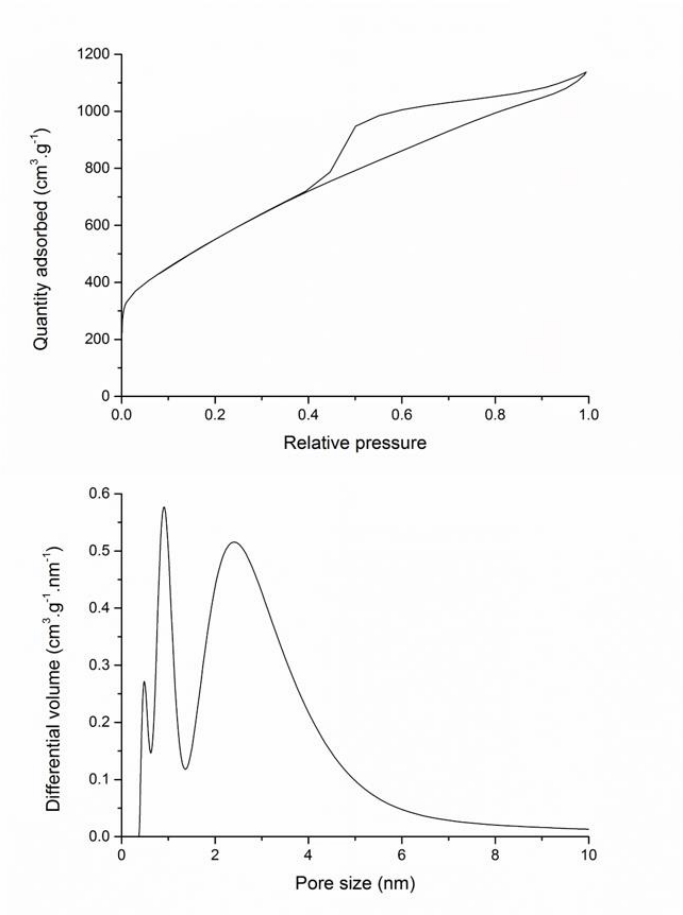
Quantity adsorbed (cm^3.g^{-1})
Relative pressure
Differential volume (cm^3.g^{-1}.nm^{-1})
Pore size (nm)

Fig 3

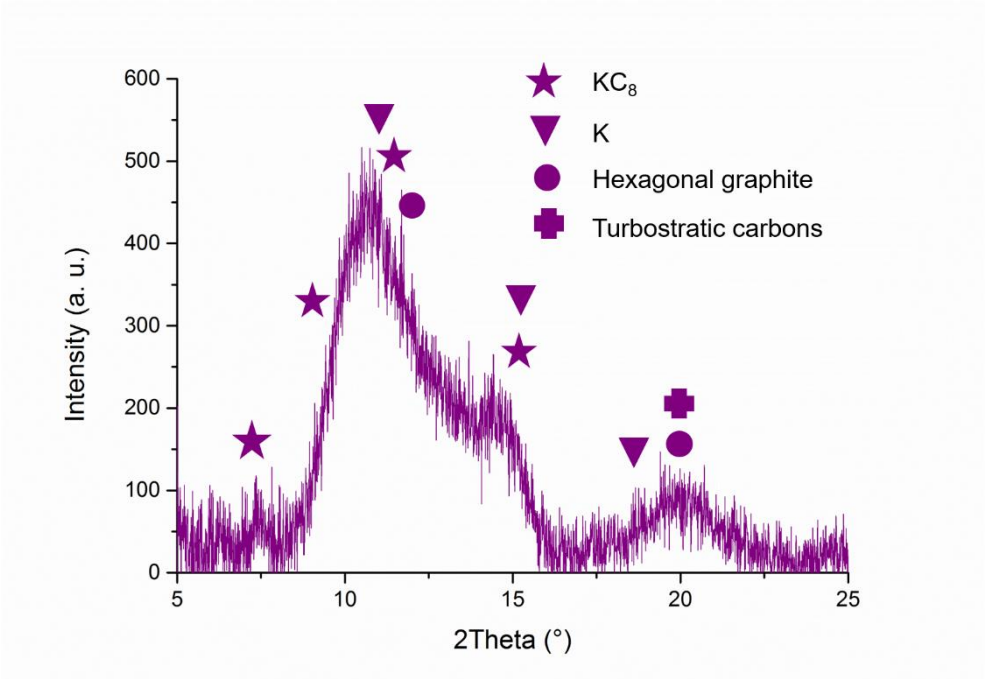
KC$_8$
K
Hexagonal graphite
Turbostratic carbons
Intensity (a. u.)
2Theta (°)

Fig 4

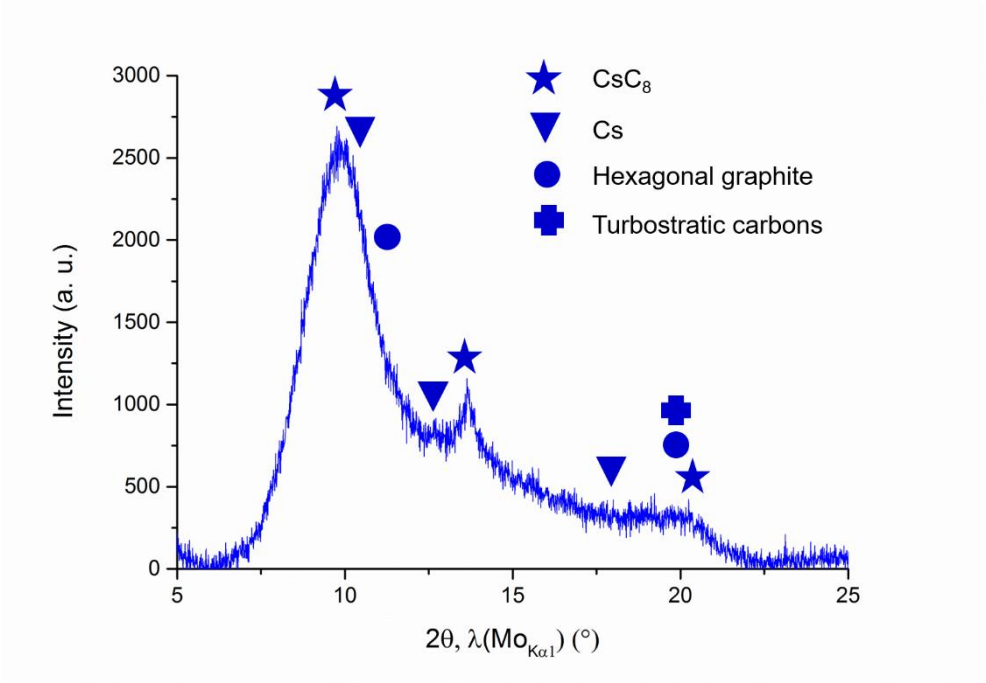
3000
2500
2000
1500
1000
500
0
5
10
15
20
25
Intensity (a. u.)
2θ, λ(Mo$_{Kα1}$) (°)
CsC_8
Cs
Hexagonal graphite
Turbostratic carbons

Fig 5

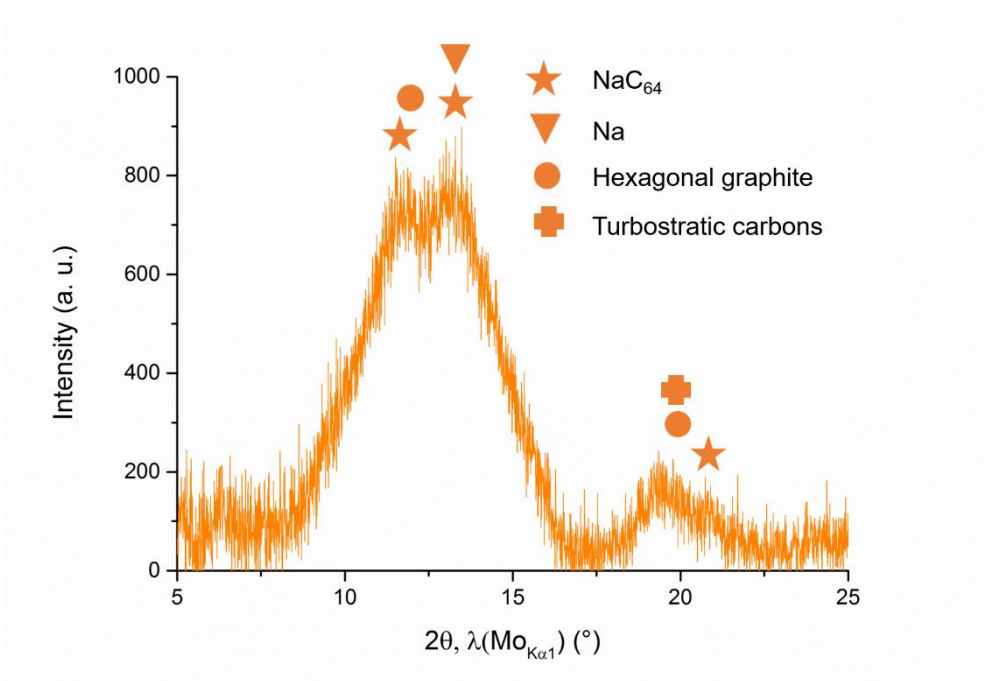
1000
800
600
400
200
0
5
10
15
20
25
Intensity (a. u.)
2θ, λ(Mo$_{Kα1}$) (°)
NaC_{64}
Na
Hexagonal graphite
Turbostratic carbons

Fig 6

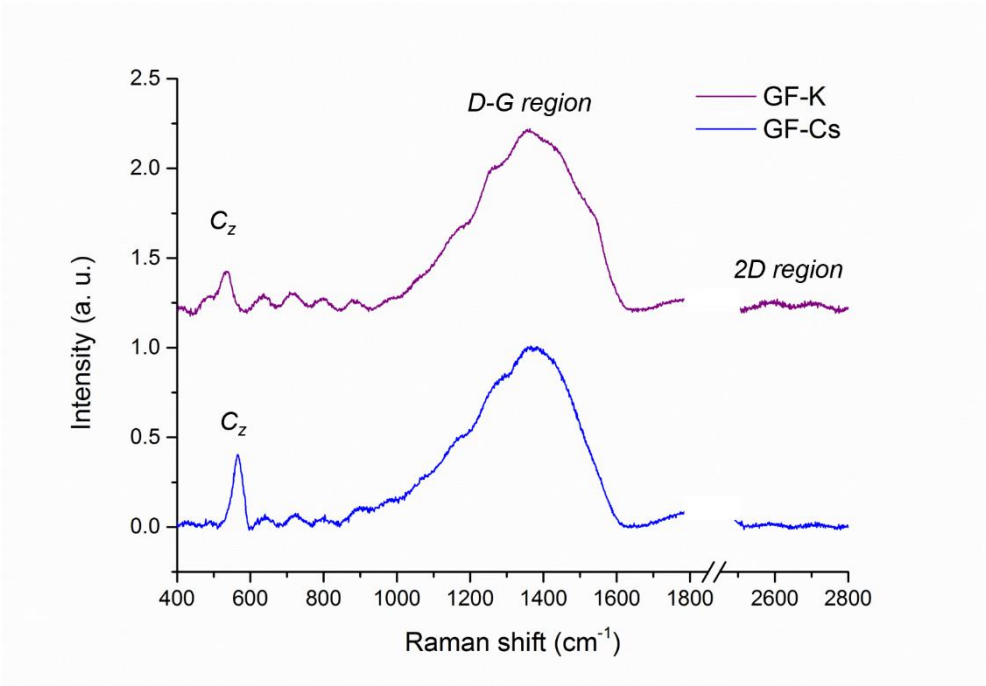
D-G region
GF-K
GF-Cs
C_z
2D region
C_z
Intensity (a. u.)
Raman shift (cm^{-1})
2.5
2.0
1.5
1.0
0.5
0.0
400
600
800
1000
1200
1400
1600
1800
2600
2800

Fig 7

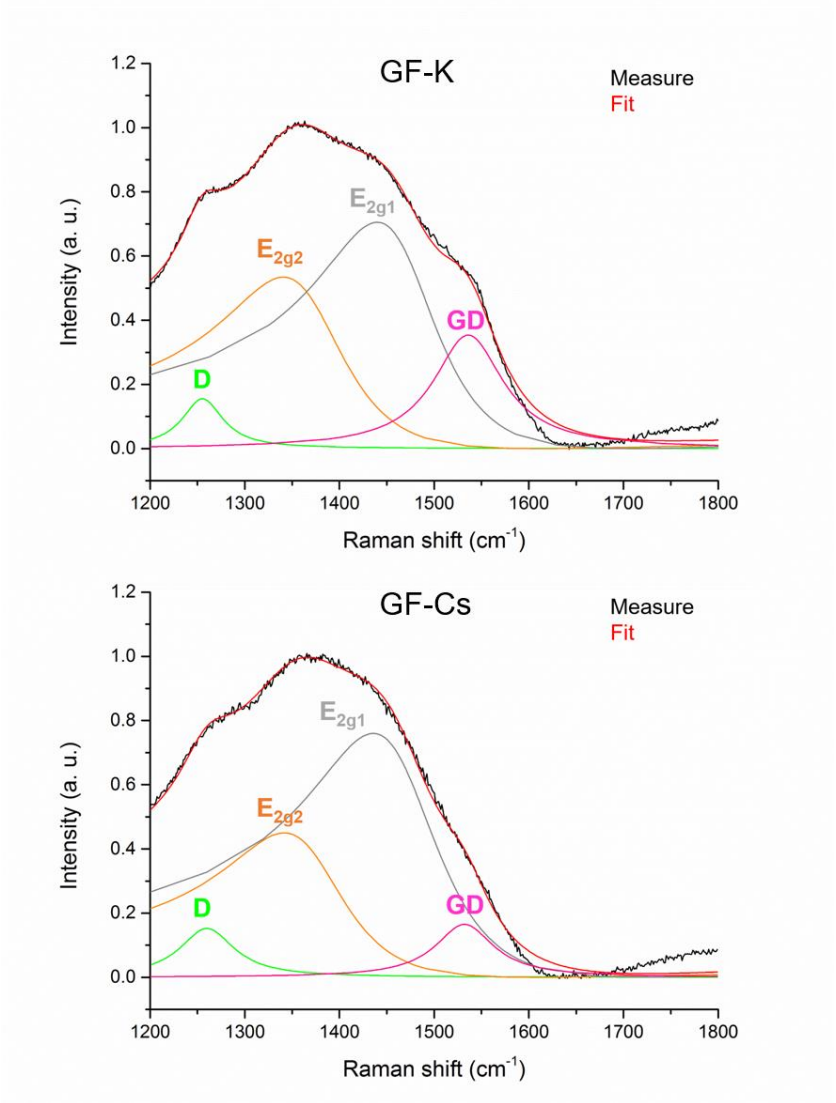
GF-K
Measure
Fit
E_{2g1}
E_{2g2}
GD
D
Intensity (a. u.)
Raman shift (cm^{-1})
GF-Cs
Measure
Fit
E_{2g1}
E_{2g2}
D
GD
Intensity (a. u.)
Raman shift (cm^{-1})

Fig 8

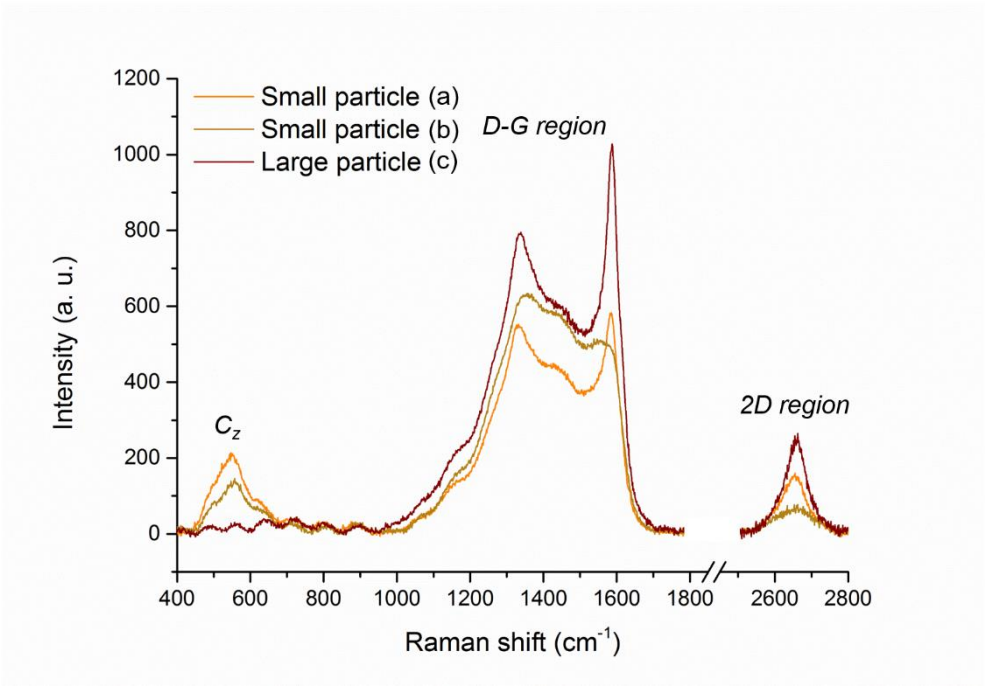
Small particle (a)
Small particle (b)
Large particle (c)
D-G region
2D region
C_z
Intensity (a. u.)
Raman shift (cm^{-1})
0
200
400
600
800
1000
1200
400
600
800
1000
1200
1400
1600
1800
2600
2800

Fig 9

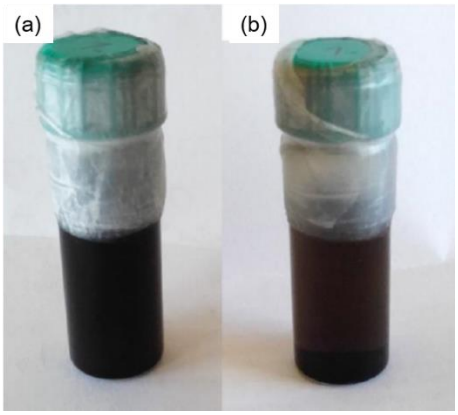
(a)
(b)

Fig 10

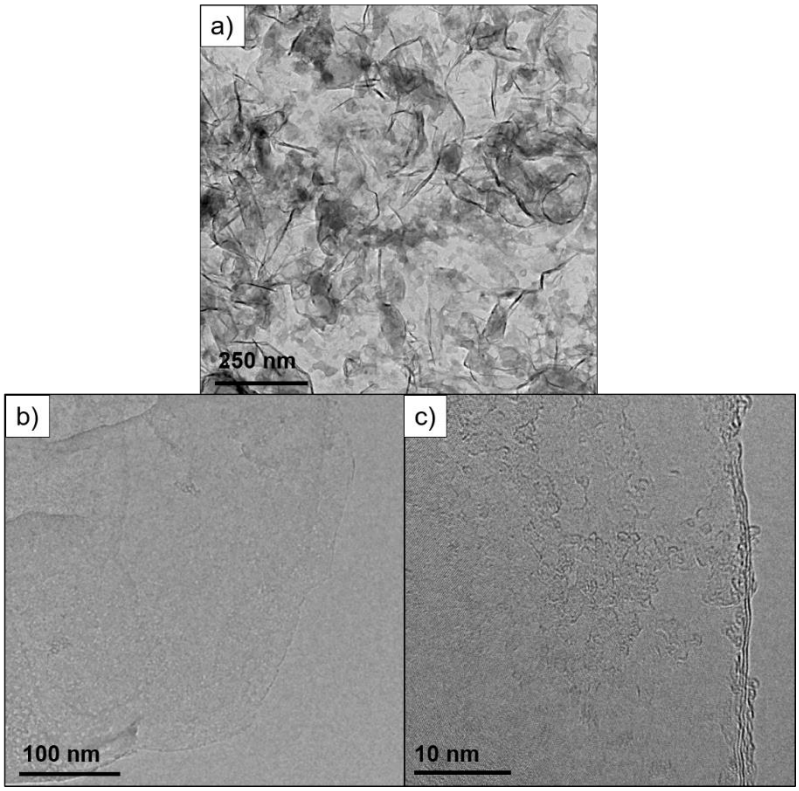

Fig 11